doi:10.1016/j.jmb.2011.04.035 J. Mol. Biol. (2011) 409, 654–668

Contents lists available at www.sciencedirect.com

Journal of Molecular Biology

journal homepage: http://ees.elsevier.com.jmb

Probing Dimerization and Structural Flexibility of Mammalian Lipoxygenases by Small-Angle X-ray Scattering

Weifeng Shang[1], Igor Ivanov[2], Dmitri I. Svergun[1], Oleg Y. Borbulevych[3], Ansari M. Aleem[4], Sabine Stehling[2], Jerzy Jankun[4,5,6], Hartmut Kühn[2] and Ewa Skrzypczak-Jankun[4]*

[1]*European Molecular Biology Laboratory, Hamburg Outstation, c/o DESY, Notkestrasse 85, D-22603 Hamburg, Germany*
[2]*Institute of Biochemistry, University Medicine Berlin-Charité, Monbijoustraße 2, D-10117 Berlin, Germany*
[3]*Department of Chemistry and Biochemistry, University of Notre Dame, 251 Nieuwland Science Hall, Notre Dame, IN 46556, USA*
[4]*Urology Research Center, College of Medicine, University of Toledo-HSC, 3000 Arlington Avenue, Toledo, OH 43614, USA*
[5]*Department of Clinical Nutrition, Medical Academy of Gdańsk, Dębinki 7, 80-211 Gdańsk, Poland*
[6]*Protein Research Chair, Department of Biochemistry, College of Sciences, King Saud University, Riyadh 11451, Kingdom of Saudi Arabia*

Received 31 January 2011; received in revised form 6 April 2011; accepted 12 April 2011
Available online 20 April 2011

Edited by R. Huber

Keywords:
mammalian lipoxygenase; small-angle X-ray scattering; thermodynamic stability; thermal motion analysis; structure–function relationship

Human lipoxygenases (LOXs) and their metabolites have a great impact on human homeostasis and are of interest for targeted drug design. This goal requires detailed knowledge of their structures and an understanding of structure–function relationship. At the moment, there are two complete crystal structures for mammalian LOX [rabbit 12/15LOX (r-12/15LOX) and human 5LOX (h-5LOX)] and a fragment of human 12LOX. The low-resolution structures in solution for various LOX isoforms have brought about controversial results. Here we explored the behavior of r-12/15LOX in aqueous solution under different conditions (salt and pH) by small-angle X-ray scattering (SAXS) and compared it with human platelet-type 12S-LOX (hp-12LOX) and h-5LOX. Thermodynamic calculations concerning the stability of molecular assemblies, thermal motion analysis [TLSMD (*t*ranslation, *l*ibration, and *s*crew rotation *m*otion *d*etection based on crystallographic temperature factor B_j)], and results of SAXS analyses brought about the following conclusions: (i) in contrast to its crystal structure, r-12/15LOX functions as a monomer that dominates in solution; (ii) it dimerizes at higher protein concentrations in the presence of salt and with increasing degree of motional freedom of the N-terminal PLAT domain, as suggested by the Y98,614→R double mutant; (iii) in aqueous solutions, hp-12LOX is stable as a dimer, in contrast to h-5LOX and r-12/15LOX, which are monomeric; and (iv) all three

*Corresponding author. E-mail address: ewa.skrzypczak-jankun@utoledo.edu.
Present address: A. M. Aleem, Biochemistry Department, College of Sciences, King Saud University, Riyadh 11451, Kingdom of Saudi Arabia.

Abbreviations used: LOX, lipoxygenase; r-12/15LOX, rabbit 12/15LOX; h-5LOX, human 5LOX; SAXS, small-angle X-ray scattering; hp-12LOX, human platelet-type 12S-LOX; PDB, Protein Data Bank.

mammalian isozymes show a high level of flexibility not only for the PLAT domain but also for other subdomains of the catalytic part in TLS (*t*ranslation, *l*ibration, and *s*crew rotation) analysis and hp-12LOX in SAXS.

Introduction

Human lipoxygenases (LOXs) are of biological interest because of their involvement in physiological homeostasis and in the pathogenesis of many diseases (Refs. [1-6] and references therein). Despite years of efforts and a comprehensive functional characterization of various human LOX isoforms, their structural biology has not been well developed. X-ray coordinates have only been available for a fragment of human platelet-type 12S-LOX (hp-12LOX) [Protein Data Bank (PDB) ID: 3L3D]; however, recently, the crystal structure of human 5LOX (h-5LOX) was solved, albeit engineered and with an altered PLAT domain (PDB ID: 3O8Y).[7] Nevertheless, despite current advancements, much of our knowledge of the structural biology of human LOXs originates from homology studies based on the X-ray high-resolution structures of plant LOXs (sLOX-1, PDB ID: 1YGE; LOX-3, PDB IDs: 1RRH and 1RRL; vegetative soybean LOX-B, PDB ID: 2IUJ; vegetative soybean LOX-D, PDB ID: 2IUK), the coral 8R-LOX (PDB ID: 2FNQ), and the rabbit 12/15LOX (r-12/15LOX; PDB ID: 2P0M). All enzymes subjected to X-ray so far constitute single polypeptide chain proteins and contain 1 mol of nonheme iron per mole of enzyme as essential cofactor. Since the X-ray structure of the hp-12LOX fragment lacks the coordinates for a large number of amino acids and contains additional sequences originating from expression vectors, r-12/15LOX and h-5LOX are the only mammalian enzymes for which complete three-dimensional structures are known. Since r-12/15LOX is comparable in size to human LOX isoforms, it constitutes a suitable candidate for homology modeling of human isoforms. Although the degree of sequence identity with human enzymes is rather variable (ranging from 81% to 31%), the sequence similarity scores suggest a high degree of overall structural similarities.[8]

The X-ray structures of plant LOXs described the compact molecules, and small-angle X-ray scattering (SAXS) data[9] and dynamic fluorescence studies[10] on s-LOX1 showed rigid and compact molecules as well. On the other hand, the crystal structure of r-12/15LOX, previous SAXS measurements on r-12/15LOX[11] and hp-12LOX,[12] and dynamic fluorescence data on r-12/15LOX[10] suggested at least three elements of structural flexibility for mammalian LOX isoforms. (i) Global structural flexibility: the crystal structure of the r-12/15LOX–inhibitor complex shows relatively high temperature factors (B_{avg} = 48 Å^2) for a structure determined at −190 °C,[13] and dynamic fluorescence studies and measurements of fluorescence resonance energy transfer suggested a high degree of global conformational flexibility.[10] (ii) Interdomain movement: the N-terminal β-barrel domain (PLAT) of r-12/15LOX might swing away from the catalytic domain, as suggested by previous SAXS measurements on the recombinant enzyme and its N-terminal truncation mutant.[11] Although the SAXS data can be interpreted in a different way,[14] more recent molecular dynamics simulation confirmed the principal possibility of such interdomain motion in solvated r-12/15LOX.[15] For the solution structure of hp-12LOX, a similar movement of the PLAT domain was reported.[12] In contrast, such interdomain movement was not observed for s-LOX1.[9] (iii) Alternative molecular conformation: employing protein–ligand docking techniques and molecular dynamics simulations, we have reevaluated the original X-ray coordinates for the r-12/15LOX–inhibitor complex, and the results suggested that the enzyme undergoes conformational changes upon ligand binding,[16] as reported by Choi *et al.*[13] Helices surrounding the active site, especially surface helix 2, appear to relocate upon substrate binding to make room for incoming substrates or competitive inhibitors.

Although the crystal structure of r-12/15LOX indicated the principal possibility of dimerization,[13] its low-resolution solution structure suggested that the majority of the enzyme may be present as catalytically active monomer in aqueous solutions.[11] In contrast, hp-12LOX appears as a catalytically active dimer in aqueous solutions with a tendency to aggregate into larger oligomers.[12] The existence of Cys residues with predicted surface exposure suggested that enzyme oligomerization might be driven by the formation of intermolecular disulfide bridges, but SAXS analysis confirmed dimer stability under reducing conditions. Moreover, replacement of surface cysteines (7C/S-12LOX) did not impact dimerization but prevented oligomer formation even under nonreducing conditions.[12]

The abovementioned differences between hp-12LOX and r-12/15LOX prompted us to explore the intrinsic flexibility and molecular association behavior of these two LOX isoforms in more detail. First, we performed thermal motion analysis on r-12/15LOX based on its X-ray structure (PDB ID:

Table 1. Comparison of parameters[17] for selected interfaces in the dimers of r-12/15LOX and hp-12LOX

LOX	Dimers	Number of residues	Area [Å^2][a]	ΔG^{int} interface[b] [kcal/mol]	ΔG^{diss} dissociation[c] [kcal/mol]	Comments
r-12/15LOX (PBD: 2P0M)						
TOP-to-TOP[d]	A:B[e]	37:33	1335	−25	10	Thermodynamically stable dimer (CSS=0.5)[f]
BACK-to-BACK[d]	A:B[e]	26:31	899	−10	−1	Thermodynamically unstable ($\Delta G<0$; this model may or may not exist because of a ΔG error of 2–5 kcal/mol) (CSS=0.036)
h-5LOX (PDB ID: 3O8Y)						
BACK-to-BACK	A:B	33:33	894	−6		Thermodynamically unstable (CSS=0)
hp-12LOX (complete protein; homology model based on PDB IDs: 2P0M and 3D3L)						
TOP-to-TOP[d]	A:B	42:37	1501	−23	10	Thermodynamically most stable dimer (original homology model)
TOP-to-TOP	A:A	14:15	741	−12		This dimer has an ideal 2-fold symmetry
TOP-to-TOP	B:B	33:22	1155	−20		This is a pseudo-symmetric dimer with an arbitrary interface to increase contact between monomers *via* aromatic residues
BACK-to-BACK[d]	A:B	21:22	552	0.7		Thermodynamically unstable ($\Delta G<0$)
hp-12LOX (incomplete catalytic subunit only; PDB ID: 3D3L)						
	A:B[g]	32:32	1358	−29	−6	Thermodynamically unstable ($\Delta G<0$)

The iron for all structures and RS7 ligand in 2p0m were excluded.

[a] The numbers given represent the average contact area between the residues of monomers represented by A molecules and the residues of monomers represented by B molecules.

[b] Represents the solvation free-energy gain upon interface formation.

[c] Represents the free-energy barrier of assembly dissociation.

[d] TOP and BACK refer to the orientation of the monomers within an associated dimer (see Fig. 1a).

[e] For r-12/15LOX, molecule A represents the 'open' conformer, and molecule B represents the 'closed' conformer.

[f] CSS refers to the complexation significance score, which ranges from 0 to 1 as interface relevance to complexation increases. The dimer stability increases with an increase in the area of contact, a decrease in ΔG^{int}, and an increase in ΔG^{diss} and CSS score. This program (PISA[17]) does not consider identical molecules as assembly, or molecules with little contact at the interface; therefore, some numbers cannot be given.

[g] Here monomers A and B are two molecules present in the 3D3L structure that form an asymmetric dimer.

2P0M) and checked the thermodynamic stability of possible dimer combinations. These results were then employed for interpretation of SAXS measurements. From the new SAXS data obtained under different experimental conditions (variations of pH and salt concentrations), we concluded the solution structures of wild-type r-12/15LOX and selected mutants. Next, we compared the solution structure of wild-type hp-12LOX with that of a mutant, in which all surface-exposed cysteines were replaced by serines. Finally, we reexamined previous and new SAXS data on r-12/15LOX and hp-12LOX to quantify the degree of motional flexibility employing optimized evaluation tools.

Results

Thermodynamic stability of LOX dimers

The structure of the r-12/15LOX–inhibitor complex shows crystallographic dimers, and each dimer consists of two structurally different monomeric conformers A and B. Conformer A defines the structure of the inhibitor-free 'open' molecule, whereas conformer B represents the inhibitor-bound 'closed' LOX. Thus, for modeling, there are three principal options for dimer formation: (i) A:A, in which both monomers are 'open'; (ii) B:B, in which both monomers are 'closed'; and (iii) A:B, in which the dimer contains both conformers. The numerous theoretical options for the associations of conformers A and B into dimers have previously been discussed,[12] and the results of our free-energy calculations (Table 1) suggested that the TOP-to-TOP A:B configuration of r-12/15LOX is thermodynamically most stable.

The crystal structure of h-5LOX shows BACK-to-BACK crystallographic dimer, but the analysis of protein interfaces has not revealed any specific interactions that could result in the formation of a stable quaternary structure.

For hp-12LOX, there is no complete set of X-ray coordinates, and the available partial X-ray data do not allow reliable thermodynamic calculations. Therefore, all thermodynamic calculations on hp-12LOX were performed on a homology model based on the coordinates for r-12/15LOX. This homology model also yielded the most favorable energetic parameters

Table 2. Average *B*-factors in the rigid-moving groups of conformers A and B in the TOP-to-TOP A:B dimer upon refinement of the crystal structure (PDB ID: 2P0M) without and with TLS components

	B-factors								
moving groups	Overall	Residues 2–47	Residues 48–146	Residues 147–198	Residues 199–240	Residues 241–355	Residues 356–563	Residues 564–601	Residues 602–663
Conformer A									
2P0M[a]	50.0	67.4	52.3	51.4	49.1	40.7	41.6	51.7	45.7
No TLS (all)[b]	48.4	60.2	50.9	57.5	49.1	37.5	36.3	47.7	47.7
TLS 2[c]	30.2	28.3	25.3	39.3	35.7	24.9	25.5	35.9	26.6
TLS multi[d]	25.1	19.5	26.0	22.6	28.0	25.2	26.7	27.6	25.4

	B-factors					
moving groups	Overall	Residues 2–148	Residues 149–212	Residues 213–549	Residues 550–600	Residues 601–663
Conformer B						
2P0M	52.1	61.8	67.6	40.9	41.0	49.3
No TLS (all)	49.4	54.1	70.2	37.0	42.4	43.2
TLS 2	30.8	25.2	49.2	24.4	29.4	26.0
TLS multi	23.4	27.4	16.6	26.6	23.1	26.2

[a] PDB-deposited data; refinement with CNS, no TLS applied, includes water and inhibitor.
[b] PDB-deposited coordinates; molecules of water and inhibitor removed, all B_j values reset to 20 Å^2, and refinement performed with CCP4 6.1, Refmac5.5.0066 with auto weights, and no TLS to have a basis for this comparison.
[c] TLS 2: two *r* groups for both A and B molecules (residues 2–146 and 147–663+Fe) imitating PLAT (with flexible link) and the ellipsoidal rest of the molecule.
[d] TLS multi: with groups as in this table:

	no TLS	→	TLS 2	→ TLS multi:
R-factor(R_{free}) [%]:	21.3 (26.3)	→	20.6 (25.6)	→ 21.0 (25.5)
B_{avg} [Å^2] for all atoms:	48.9	→	27.8	→ 25.6

(Table 1) for the TOP-to-TOP A:B dimer. In the crystals formed by the engineered fragments of hp-12LOX (PDB ID: 3D3L), the molecules are joined in the asymmetric dimer that shows a negative dissociation energy ($\Delta G^{diss} < 0$; Table 1). Thus, such asymmetric dimers may not be stable in aqueous solutions.

Thermal motion analysis (TLSMD)

To test the structural flexibility of the two conformers A and B, we refined the X-ray structure of r-12/15LOX using TLS (*t*ranslation, *l*ibration, and *s*crew rotation) thermal motion analysis. Following the criteria recommended by the program, we split the two conformers into eight moving groups (conformer A) and five moving groups (conformer B), as listed in Table 2 (also illustrated in Fig. 2c). The 'open' A-conformer exhibits a higher degree of motional flexibility when compared with the 'closed' B-conformer. Incorporation of the TLS parameters only induced minor changes in the crystal structure discrepancy factors R and R_{free} [21.3 (26.3)→21.0 (25.5)], although we observed a significant decrease in B_{avg} (48.9→25.6 Å^2), where B parameters in all groups converged to levels commonly observed for cryogenic data. The same analysis performed on h-5LOX (PDB ID: 3O8Y; like rabbit 2P0M, this structure was also determined under cryogenic conditions at 100 K) indicates five possible groups with the split at N_t–122 | 123–170 | 171–355 | 356–610 | 611–673, which correspond roughly to (see Fig. 2) PLAT | LINK | TOP+PDZ | catalytic helical bundle | last helices on the front surface+tail to C_t (which is bound to Fe cofactor). These findings suggest that structural flexibility may be a true property of mammalian LOXs.

SAXS analysis

Human platelet 12LOX

As suggested by previous SAXS measurements, hp-12LOX is present in aqueous solutions as a catalytically active dimer, and here we confirmed a similar structure of the scattering solute for its 7C/S mutant. There is a good agreement between the experimental data and scattering curves calculated based on the rigid-body refined dimeric model (Fig. 1a). The linear Guinier plot (Fig. 1b) indicates that the aqueous solution was monodispersive, and the scattering solutes yielded a radius of gyration R_g of 49±2 Å. The volume of the scattering solutes was (300±10)×10^3 Å^3, corresponding to a molecular mass of 150±5 kDa, which is twice the molecular mass of the enzyme monomer (75 kDa). These results indicate that the wild-type enzyme forms stable dimers in solution. Its 7C/S mutant yielded identical R_g values and molecular masses, as well as similar scattering profiles (data not shown). Thus, a Cys-to-Ser exchange of surface residues did not cause major alterations in dimer size and shape. For both enzyme species, the maximum size of the solute particle D_{max}

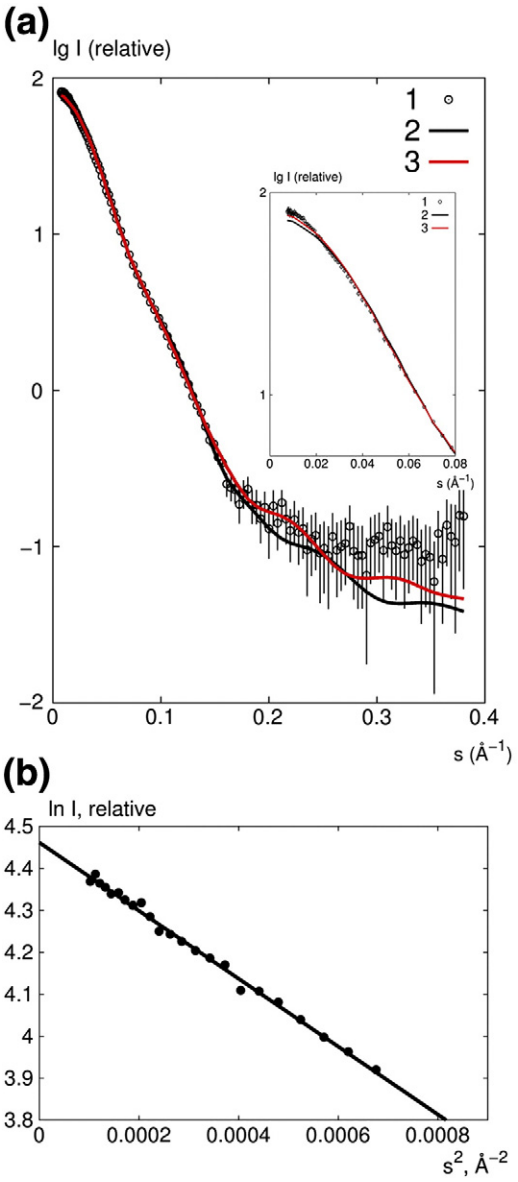

Fig. 1. SAXS patterns of hp-12LOX. (a) Scattering patterns of wild-type hp-12LOX (1) and fits of the three-group rigid-body models (2) and the five-group rigid-body models (3). The logarithms of the scattering intensity were a function of the momentum transfer $s=4\pi\sin\theta/\lambda$, where 2θ is the scattering angle and λ is the X-ray wavelength. Inset: Enlarged view of the low s region. (b) Guinier plot (linear dependence of the natural logarithm of the intensity on the square of the momentum transfer) indicates monodispersity of the enzyme solution.

was 165 ± 5 Å. In comparison, the crystal structure of the r-12/15LOX–inhibitor dimer yielded significantly smaller R_g (41.2 Å) and D_{max} (145 Å) values, and these data might be related to a different degree of motional flexibility. These differences prompted us to further explore the structural flexibility of both enzymes employing rigid-body modeling.

First, we studied the flexibility of hp-12LOX using the previous SAXS low-resolution model[12] but allowing more freedom of motion for different moving groups, which were defined as follows: (i) PLAT domain (residues 1–108), (ii) PDZ domain (residues 224–334), and (iii) a bundle of helices of the catalytic domain (residues 109–223 + 335–663 containing iron). The catalytic parts forming the interface were treated jointly as one group in the three-group and five-group models, while they were allowed to move as independent entities in the four-group and six-group models. The discrepancy values χ between the experimental curves and the calculated curves of the individual SASREF runs are given in Table 3. In general, χ decreased with increasing degrees of motional freedom. It somewhat decreased when catalytic domains were allowed to move relative to each other (four groups per dimer), but significant improvement was observed when the bulk catalytic domain was split and the PDZ domain was introduced (five groups per dimer), as illustrated in Fig. 1a. This procedure allows χ to approach 1, indicating optimal fitting. Figure 2b depicts the refined model (six groups per dimer) showing all atoms over the calculated envelope of the scattering solute. Figure 2c illustrates the results of TLS analysis with molecules in the same orientation. The following properties of the biologically active LOX dimer were concluded: (i) the two monomers appear to be structurally different; (ii) they carry independently moving PLAT domains (interdomain movement); (iii) they contain a flexible catalytic core, and the degree of flexibility could be controlled by more than two groups of the tertiary structure; and (iv) the interdomain movement between PLAT and the rest of the monomer is not the only kind of motional flexibility of hp-12LOX, and the dimer might undergo adjustments in the relative orientation of its individual molecules and their domains and subdomains.

Rabbit 12/15LOX

Previous SAXS measurements on r-12/15LOX indicated considerable mismatches between theoretical scattering patterns calculated based on the crystal structure and the experimental SAXS data. This mismatch was most pronounced in the region of the N-terminal PLAT domain and was not detected for the PLAT domain truncation mutant.[11] These results have alternatively been interpreted, with interdomain movement and/or protein dimerization[14] suggested as structural basis. Here we recorded the scattering profiles of recombinant wild-type r-12/15LOX under different experimental conditions and included both options in the evaluation algorithm of the SAXS data.

Table 3. Discrepancy factors χ calculated from the SAXS data measured for wild-type hp-12LOX and its 7C/S mutant

Enzyme species	Three moving groups per dimer[a]	Four moving groups per dimer[b]	Five moving groups per dimer[c]	Six moving groups per dimer[d]
Wild-type hp-12LOX	1.63[e]	1.33	1.05[e]	0.99[f]
7C/S mutant	2.70	2.02	1.15	1.06

For refinement of the structural models, the monomeric components of the A:B dimers were divided into three rigid-moving groups (PLAT domain, PDZ domain, and CAT domain), as indicated in Fig. 2a. The PLAT domain comprises residues 1–108, the PDZ domain comprises residues 224–334, and the CAT domain comprises residues 109–223 + 335–663, including nonheme iron. A discrepancy factor of 1 means structural identity.

[a] Rigid-moving groups: PLAT in conformer A, CAT in conformers A + B, and PLAT in conformer B.

[b] Rigid-moving groups: PLAT in conformer A, CAT in conformer A, PLAT in conformer B, and CAT in conformer B.

[c] Rigid-moving groups: PLAT in conformer A, PDZ in conformer A, CAT in conformers A + B, PDZ in conformer B, and PLAT in conformer B.

[d] PLAT in conformer A, PDZ in conformer A, CAT in conformer A, PLAT in conformer B, PDZ in conformer B, and CAT in conformer B.

[e] The fits of three-group and five-group models are shown in Fig. 1a.

[f] This dimer model is shown in more detail in Fig. 2b.

Impact of pH and enzyme concentration on the solution structure. Initially, we determined the SAXS patterns at pH 6.8 and pH 8.0 in the absence of salt (20 mM Tris–HCl). These pH values were chosen since they flank the physiological range and might correspond to membrane-associated and cytosolic conformers of the enzyme.[18] Moreover, CD-based stability measurements indicated a high degree of protein stability under these conditions. From Fig. 3a, it can be seen that the experimental scattering patterns predicted based on the crystal structure (chain A in PDB ID: 2P0M) fairly match the experimental data at low

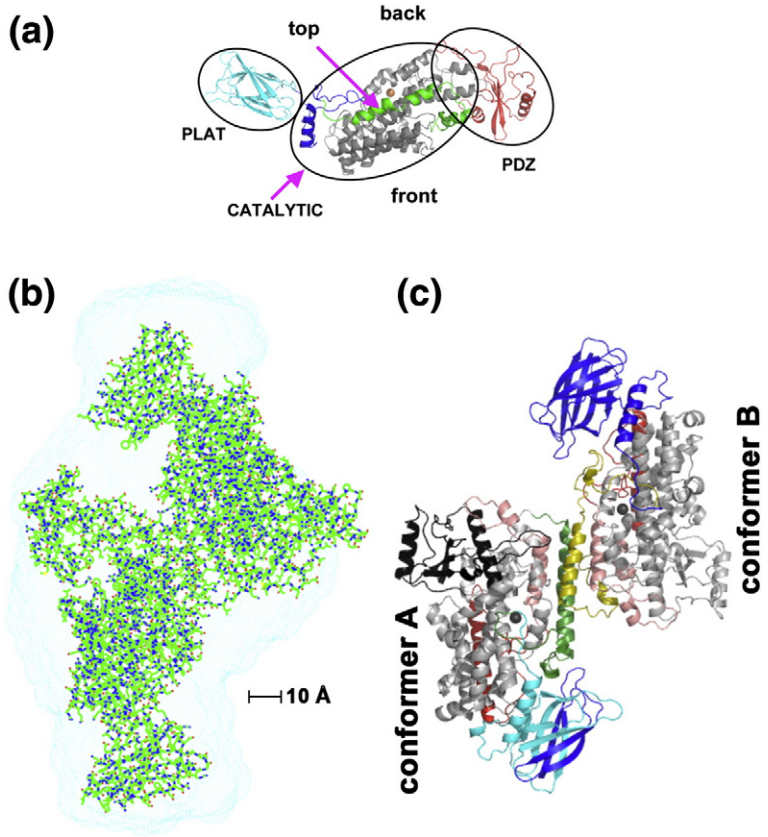

Fig. 2. Refined model for the solution structure of hp-12LOX. (a) The monomers were subdivided into three groups used in SAXS rigid-body refinement: (i) the PLAT domain comprising residues 1–108, (ii) the PDZ domain comprising residues 224–334, and (iii) the CAT domain comprising residues 109–223 + 335–663, including nonheme iron. (b) Dynamic model of the solution structure (six independently moving groups; see Table 3) of hp-12LOX dimer. (c) Ribbon model of the 2P0M crystal structure showing (in different colors) eight groups in monomer A and five groups in monomer B, as used in thermal motion analysis (TLSMD; see Table 2).

protein concentrations. However, at higher concentrations, significant mismatches were observed (Fig. 3b). A more detailed evaluation of all sets of scattering data recorded at different enzyme concentrations and pH in the presence and in the absence of salt suggests a polydispersive character of the enzyme solution. The R_g values (radius of gyration) calculated from the scattering curves and plotted against the protein concentration (Fig. 4a) show a linear increase in R_g values with increasing protein concentrations at pH 6.8. Since data sets showing signs of nonspecific protein aggregation were eliminated, these observations suggested a monomer–dimer equilibrium, and the equilibrium was shifted toward dimer formation with increasing concentrations. At pH 8.0, such shift was not observed.

Considering the results of rigid-body refinement for interpretation of the scattering data, we have calculated the monomer–dimer ratios and the discrepancy factors χ (Table 4). To structure this table, we first assumed that the molecular dimensions of enzyme monomers and enzyme dimers in aqueous solutions and in the crystals are identical (no interdomain movement), and then we calculated the monomer–dimer ratio, which best fitted the experimental scattering patterns. Next, we allowed the motional flexibility of the N-terminal PLAT domain and recalculated the monomer–dimer ratio. Comparison of these two monomer–dimer ratios indicated no major differences between the two methodological approaches, suggesting that interdomain movement may be minimal in the absence of salt. These results have also indicated that, even at high protein concentrations, rabbit LOX monomers are the dominating enzyme species (>78%). This conclusion is in contrast to the findings on hp-12LOX, which occurs as dimers in aqueous solutions. The existence of larger LOX oligomers in these samples was ruled out by the SAXS data gel filtration and native gel electrophoresis. Owing to the low atomic resolution (25 Å) of our SAXS data, we found it impossible to determine which conformer (A-open or B-closed) was dominating.

Impact of salt. Since ionic interactions might be important for protein dimerization, higher salt concentrations should impact the scattering patterns. Indeed, when SAXS measurements were carried out in the presence of near-physiological salt concentrations (200 mM NaCl), the R_g values were strongly increased (Fig. 4a), and the share of dimers rose to about 25% at pH 6.8 and to 35% at pH 8. Moreover, in the calculated rigid-body refined models, the PLAT

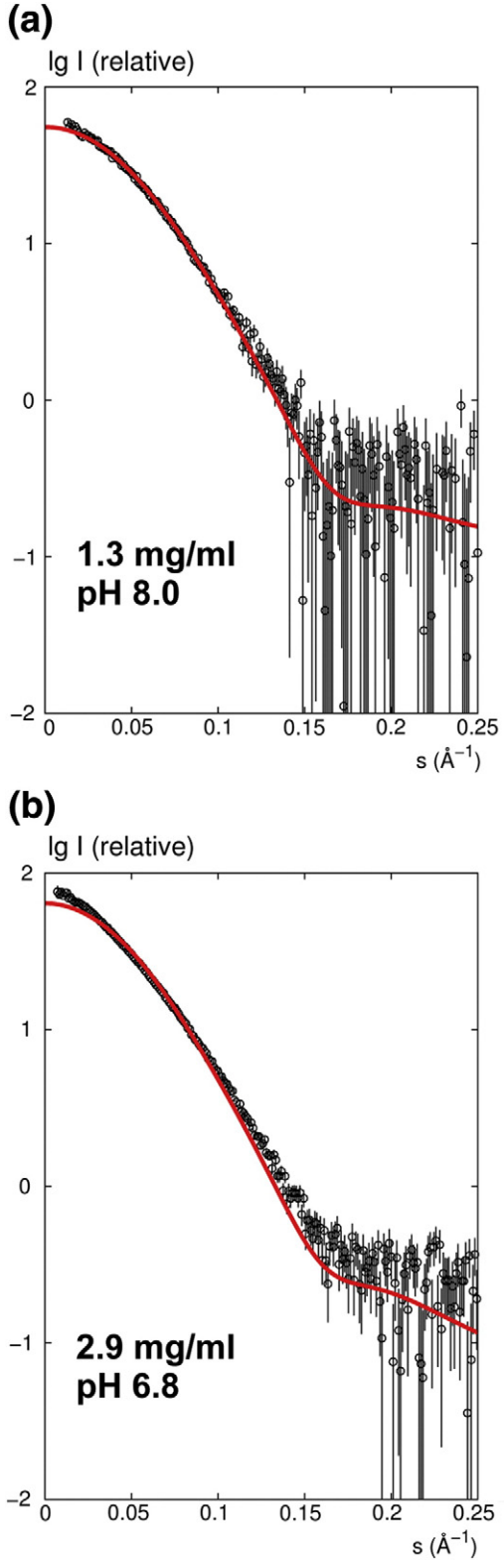

Fig. 3. SAXS patterns of r-12/15LOX. Black traces represent the experimentally obtained scattering patterns. The red line indicates theoretical scattering curves calculated based on the crystal structure. (a) Scattering patterns of wild-type r-12/15LOX in 20 mM Tris–HCl buffer (pH 8) (1.2 mg/ml). (b) Scattering patterns of wild-type r-12/15LOX in 20 mM Tris–HCl buffer (pH 6.8) (2.9 mg/ml).

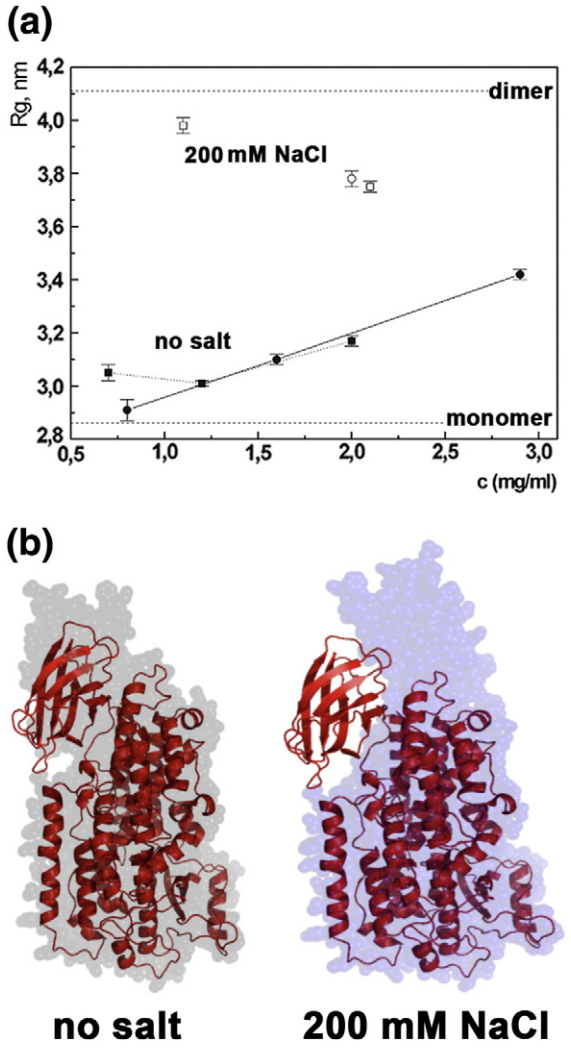

Fig. 4. Impact of salt and enzyme concentration on the solution structure of r-12/15LOX. SAXS measurements for wild-type r-12/15LOX were carried out in 20 mM Tris–HCl (pH 6.8) in the presence and in the absence of 200 mM NaCl. (a) The radii of gyration (R_g) representing the size of the molecule under different experimental conditions were extracted from the original SAXS data. (b) The solution structures are represented by colored silhouettes, and the crystal structure is overlaid as the ribbon model for comparison.

domain appears to swing away from the catalytic domain, resulting in significant expansion of the enzyme molecule (Fig. 4b). Thus, our SAXS data recorded in the presence of salt suggest interdomain movement in addition to dimer formation.

Mutation at the interdomain interface. When we inspected the interdomain interface between the PLAT domain and the catalytic subunit of r-12/15LOX, we found that Y98 of the PLAT domain might form a π-electron sandwich with Y614 of the catalytic domain (Fig. 5a). This noncovalent interaction might contribute to limit interdomain movement in the absence of salt. To confirm the importance of such stacking interaction, we mutated these two Y residues to positively charged *R*, expecting that lack of π–π interactions and introduction of electrostatic repulsion forces may increase the PLAT domain movement. The scattering patterns of wild-type and mutant enzyme species (Table 5) were found to have similar R_g values of 31.9 Å and 32.7 Å for the wild-type r-12/15LOX and its Y614R mutant. However, for the Y98R + Y614R double mutant, a significantly increased R_g value (38.5 Å) was observed. These data suggest that single mutation might not be sufficient to induce a higher degree of interdomain movement, but that electrostatic repulsion of the two introduced arginines may force separation of the PLAT domain from the rest of the molecule.

This conclusion was confirmed by independent gel-filtration studies (Fig. 5B). Here, wild-type r-12/15LOX and its Y614R mutant eluted with a hydrodynamic radius (R_h) of 30.8 Å, whereas the Y98R + Y164R double mutant eluted with an R_h of 34.1 Å.

When we evaluated the scattering data by employing our rigid-body refined structure model (Fig. 5C), we also found that Y614R exchange may not be sufficient to induce significant interdomain movement, as indicated by the fair match of crystal and solution structures. However, for Y98R + Y614R, there is significant elongation of the longitudinal axis of the molecule, suggesting that under these experimental conditions, the PLAT domain may swing away from the catalytic subunit. In fact, the overall shape of the solution structure of this double mutant in the absence of salt resembles that of the wild-type enzyme at higher salt concentration (Fig. 4b). Moreover (data not shown), the share of enzyme dimers in the absence of salt significantly increased from 7% (wild-type enzyme) *via* 13% (Y614R) and to 27% (Y98R + Y614R) (Table 5).

Low-resolution structure of r-12/15LOX dimers. As indicated in Table 4, the refined model for the solution structure of r-12/15LOX has suggested that at pH 6.8 in the absence of salt, the vast majority of the enzyme is present as hydrated monomer, but the share of enzyme dimers increases with increasing protein concentrations. To obtain information on the structure of r-12/15LOX dimers, we created an *in silico* model for the enzyme dimer that exhibits *P*2 symmetry. In this model, the surface-exposed H2 helices of the two monomers contact each other. Since the atomic resolution of our SAXS data was only about 30 Å, we could not distinguish between A-open conformers and B-closed conformers. In Fig. 6b, the crystal structure of these dimers was overlaid by their solution structures. In the absence of salt, we observed a fair match of crystal and solution structures for the wild-type

Table 4. Share of enzyme monomers and dimers in aqueous solutions of r-12/15LOX

		Crystal structure model			Refined solution structure model		
pH	*c* [mg/ml]	χ	Share of monomers [%]	Share of dimers [%]	χ	Share of monomers [%]	SHARE of dimers [%]
6.8	0.8	2.69	90	10	2.69	92	8
	1.6	1.41	87	13	1.27	88	12
	2.9	1.73	78	22	1.34	78	22
8.0	0.7	1.10	87	13	1.06	87	13
	1.2	1.10	94	6	1.07	96	4
	2	1.38	84	16	1.22	85	15

The discrepancy factor χ indicates the difference between the experimental data and the fit of a linear combination of scattering profiles estimated from the monomer–dimer equilibrium as in the crystal structure and in the refined structure.

enzyme and its Y98R mutant, suggesting minimal interdomain movement. However, as for the monomers, we also detected for the dimers a mismatch between crystal structure and solution structure for the wild-type + salt enzyme and the Y98R + Y614R double mutant in the region of the PLAT domain, and these data were interpreted as an indication for interdomain movement within the LOX dimer.

Discussion

Stability of LOX dimers in aqueous solutions

To conclude the structure of a protein in aqueous solutions from experimental SAXS data, one needs a high-resolution starting model; however, for hp-12LOX, such data are currently not available for the whole and unengineered molecule. In h-5LOX, the BACK-to-BACK dimer present in the crystal (PDB ID: 3O8Y) is not a thermodynamically stable assembly and this enzyme is predicted to perform as a monomer. Thus, we constructed a homology model for hp-12LOX based on the X-ray coordinates for r-12/15LOX (PDB ID: 2P0M) using hp-12LOX (PDB ID: 3D3L) where appropriate. Employing this strategy, we previously suggested that hp-12LOX is present in aqueous solutions as a catalytically active dimer,[12,19] contradicting previous findings on other LOX isoforms.[9,11] The crystal structure of the r-12/15LOX–inhibitor complex[13] has indicated the existence of heterodimers, in which one monomer was liganded by the inhibitor and adopted the closed conformation (conformer B) while the other was ligand-free and had the open conformation (conformer A). While the RMSD for the main chains of these two molecules is 0.5 Å in general, there are two regions where they seriously differ: (i) residues 163–215, with the surface helix 2 moved by ~12 Å, and (ii) residues 591–603, which is another surface-exposed fragment near the active site. In contrast to solid state, in aqueous solutions (in the absence of this ligand), r-12/15LOX is mainly present as a monomer. This is not unusual, since protein packing in the crystal may energetically favor dimerization.[20] It is worth noticing that the crystallization media contained 0.48 M lithium sulfate,[21] which could cause dimerization due to increased ionic strength (~7 times of what you see in Fig. 4a). Also, rapid crystal freezing can affect not only crystal lattice but also molecules, especially external loops, hydrogen bonding network, and so on, even distribution of water in the cavities.[22] In this study, we first explored, by *in silico* modeling, possible associations of conformers (A

Table 5. Comparison of the hydrodynamic radii estimated from gel filtration and the R_g values obtained by SAXS

	Gel filtration[a]	SAXS data	
Sample	R_h [Å]	R_g [Å]	Share of monomers [%]
Wild-type	30.8	31.9[b]	93
Y614R	30.8	32.7[c]	87
Y98R + Y614R	34.1	38.5[d]	73

The theoretical R_g value calculated based on the crystal coordinates is 28.4 Å. The increase in R_h for the double mutant suggests that Y98R + Y614R might exhibit a higher degree of motional flexibility, consistent with the SAXS data.

[a] SAXS sample (90–100 μg) was applied for gel filtration.
[b] Measured at the lowest concentration of 0.8 mg/ml.
[c] Measured at the lowest concentration of 0.5 mg/ml.
[d] Measured at the lowest concentration of 0.5 mg/ml.

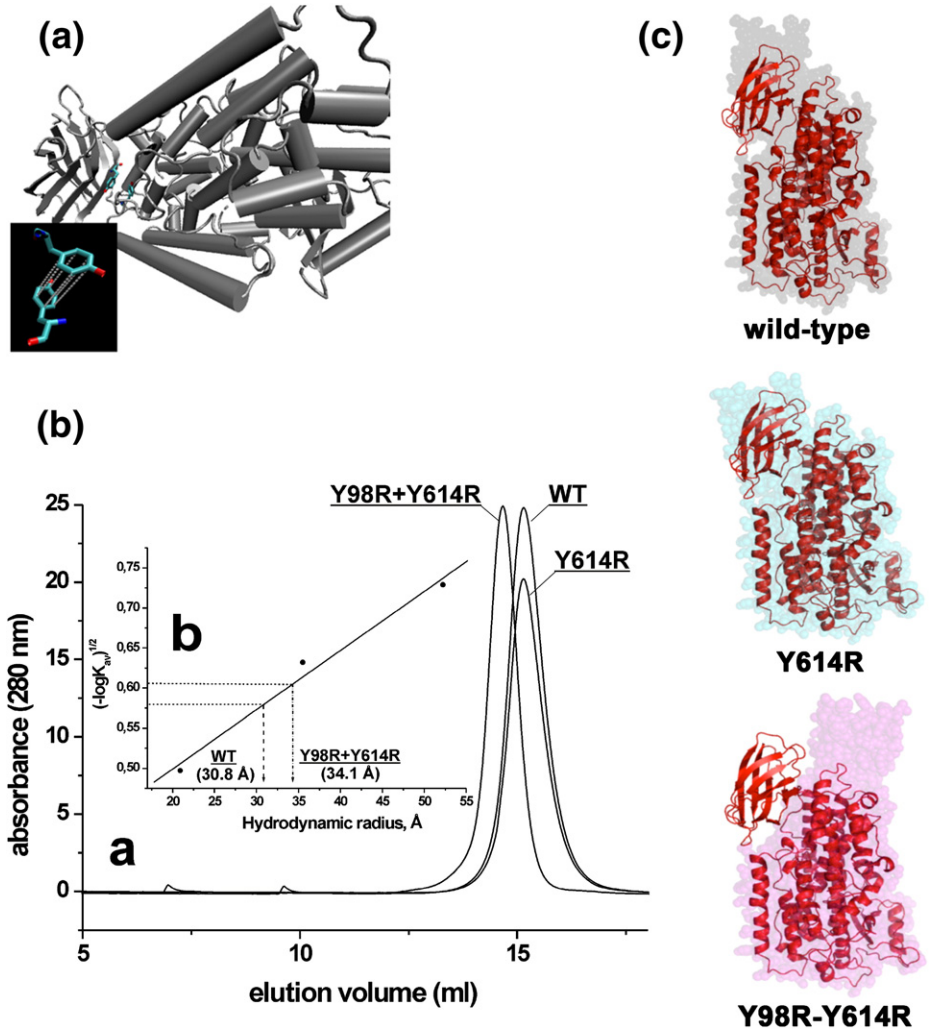

Fig. 5. Mutations at the interdomain interface force an increased degree of interdomain movement: (a) Inspection of the interdomain interface of the crystal structure shows Y98 and Y614 residues bound *via* π–π interactions and thus limiting interdomain movement. (b) **a**: Gel-filtration elution profiles for wild-type r-12/15LOX and its Y614R and Y98R + Y614R mutants indicating different elution volumes of the enzyme species. **b**: Determination of hydrodynamic radii after the calibration of the column (see Materials and Methods). (c) The solution structures calculated from the SAXS data are represented by colored silhouettes with the crystal structure as the ribbon model overlaid for comparison.

versus B) within dimers of r-12/15LOX and hp-12LOX. Analysis of theoretically possible inter-monomer interfaces suggested (Table 1) that the TOP-to-TOP model of an A:B dimer was thermodynamically most stable for both r-12/15LOX and hp-12LOX and in accordance with the shape of the scattering solute in the SAXS results for the monodispersive samples.

Solution structure of hp-12LOX

Employing thermal motion analysis, we attempted to shed light on the motional flexibility of hp-12LOX dimers occurring in aqueous solutions. Although the program suggested 8 and 5 rigid-moving groups for conformers A and B described for r-12/15LOX (13 rigid-moving groups per dimer), we have restricted our modeling on hp-12LOX to 6 rigid-moving groups per hp-12LOX dimer in a low-resolution (16 Å) model. The ab initio shape determination of the enzyme was carried out by repeated runs of the DAMMIN software package, and this procedure yielded reproducible models that were further analyzed and averaged (DAMAVER). We have concentrated on the A:B model and subdivided the polypeptide chain of each monomer into the following three rigid-moving groups (Fig. 2a): (i) PLAT domain (residues 2–108), (ii) PDZ domain (residues 224–334), and (iii) CAT domain comprising the rest of the molecule. The PLAT

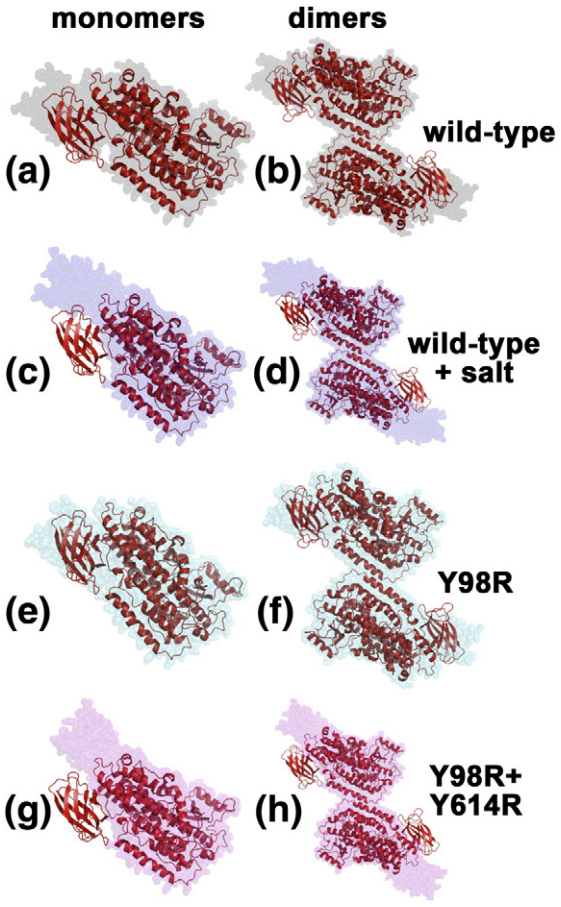

Fig. 6. (a–h) Low-resolution solution structures of the monomers and dimers of r-12/15LOX. Recombinant wild-type and mutant r-12/15LOX were prepared as described in Materials and Methods. The monomer–dimer ratio calculated from the original SAXS data is given in Table 4. Colored silhouettes represent the low-resolution solution structure with the starting model based on the crystal structure given as the ribbon diagram for comparison. The mismatch in the region of the PLAT domain, especially in the presence of salt (200 mM NaCl) and for the Y98R + Y614R double mutant, was interpreted as an indication for the independent movement of this structural subunit.

domain was free to move in all models; the three-group and five-group models had the two CAT domains arrested as in the crystal structure and were treated as one rigid moiety; while in the four-group and six-group models, A-CAT and B-CAT were allowed to move independently. In the five-group and six-group modeling, PDZ domains were added as separate entities to increase the flexibility of the bulk of each monomer. In all our models, the PLAT domain seems to adopt a random orientation (Fig. 2b), thus leading to an asymmetric shape of the dimer. There is also a noticeable difference in the catalytic part that seems to follow the pattern of thermal motion detected in conformer A (Fig. 2c). This recombinant enzyme never shows enzyme–Fe stoichiometry as 1:1, but usually 0.3–0.7 for iron (Aleem *et al.*[23] and references therein), which obviously means that apo and active molecules are concurrently present in solution. Although there is no experimental proof, we might speculate that the dimers do not have to be homodimers, but could be heterodimers consisting of apo and active molecules, and this can impact the dimer shape and behavior. Asymmetric protein dimers have been described before, and ubiquitin ligase is an example of a homodimer in which the monomers adopt completely different conformations.[24] Moreover, metamorphic proteins, which have the same primary structure but adopt different folded conformations, also indicate that different conformers may share large common substructures but differ in other parts of the protein.[25]

Solution structure of r-12/15LOX

Previous SAXS measurements on r-12/15LOX[11] and s-LOX1[9] suggested that these enzymes occur in aqueous solutions as monomers, although reinterpretation of the r-12/15LOX data suggested partial oligomerization of the enzyme.[14] When we interpreted the original SAXS data of r-12/15LOX,[11] enzyme dimerization was not considered, since, at that time, there was no experimental evidence for the existence of dimeric LOXs in aqueous solutions. Thus, the mismatch between crystal structure and solution structure was interpreted solely as a consequence of the motional flexibility of the enzyme in aqueous solutions. However, in the light of recent findings, it became clear that enzyme dimerization is a process to be considered; thus, structural flexibility and enzyme dimerization must be included in the interpretation of LOX SAXS data.

In general, the structural flexibility of proteins in aqueous solutions and protein dimerization are impacted by both protein concentrations and solution conditions, such as salt and pH. To explore the solution structure of r-12/15LOX in more detail, we employed a dual approach: (i) we collected SAXS data at various protein concentrations, different pH values (6.8 and 8.0), and different salt concentrations; and (ii) based on the X-ray coordinates, we performed rigid-body modeling using the SASREF software package.[26] Assuming a monomer–dimer equilibrium, we simultaneously fitted various experimental curves and allowed independent movement of the N-terminal PLAT domain. Finally, low-resolution models were restored from the refined monomer and dimer conformations ab initio using the DAMMIF program. Following this algorithm, we found that at pH 6.8, the share of the enzyme monomers of r-12/15LOX in aqueous solutions was

more than 90% at a protein concentration lower than 1 mg/ml. However, the share of dimers increased at higher protein concentrations, reaching 30% at about 3 mg/ml. Under these conditions, we did not observe a major interdomain movement. However, when we included salt under near-physiological conditions, the SAXS data obtained suggested that the N-terminal PLAT domain may swing away from the catalytic subunit. Thus, one may conclude that an increase in ionic strength may force interdomain movement, consistent with previous SAXS measurements on this enzyme.[11]

To probe the movement of the N-terminal PLAT domain relative to the catalytic subunit, we have mutated the tyrosine residues at the interdomain interface (Fig. 5a). To induce maximal electrostatic repulsion, we have introduced positively charged arginines on either site of the interdomain interface. SAXS data suggested that the longitudinal diameter of the Y98R + Y614R double mutant was significantly higher than that of the wild-type enzyme even in the absence of salt, suggesting that the PLAT domain may swing out farther under these experimental conditions. Thus, we concluded that simultaneous Y98R and Y614R exchange can unleash and improve the interdomain movement.

Motional flexibility might be the basis for the allosteric character of mammalian LOX

hp-12LOX and r-12/15LOX have been suggested to exhibit allosteric properties.[27,28] There is circumstantial evidence for the existence of allosteric regulatory sites, but the precise structures of these binding sites have not been clarified. Nevertheless, allosteric regulatory mechanisms require structural rearrangement. The crystallographic data suggest that ligand binding may induce major conformational alterations in r-12/15LOX.[13] Moreover, comparative fluorescence studies carried out on both r-12/15LOX and s-LOX1 suggest a high degree of the motional flexibility of r-12/15LOX.[10] The SAXS data presented here for both hp-12LOX and r-12/15LOX suggest interdomain movement under near-physiological salt concentration, joining the chain of experimental evidence suggesting motional flexibility of mammalian LOXs. Although motional flexibility constitutes the structural basis for the allosteric character of r-12/15LOX, the molecular mechanism of that allosteric regulation in r-12/15LOX remains to be worked out in the future. The case of hp-12LOX is more complicated since we have two molecules suppose to work in unison conducting the transfer and catalysis of possibly six molecules (three molecules per monomer), as was indicated by arachidonic acid binding studies.[12,23] In fact, identification of the allosteric binding sites seems to be the most important next step in the explanation of the intricate properties of mammalian LOXs.

Materials and Methods

Protein expression and purification

Recombinant wild-type r-12/15LOX and selected mutants were expressed in *Escherichia coli* as His-tagged fusion proteins.[29] Bacteria were transformed with the recombinant plasmids, and, routinely, 18 l of LB medium containing 100 mg/l ampicillin was inoculated with a 20-ml overnight preculture pro 1L medium. The bacteria were allowed to grow at 37 °C for 20 h, and then expression of recombinant protein was induced by addition of 1 mM isopropyl-β-D-thiogalactopyranoside (final concentration). The cultures were kept for an additional 3 h at 26 °C, and then the bacteria were pelleted, washed and resuspended in 60 ml of phosphate-buffered saline. Cells were disrupted using an EmulsiFlex-C5 pressure homogenizer (Avestin, Canada) at 15 MPa, and debris was spun down. The clear lysis supernatant was applied to 2 × 1.6-ml nickel-agarose columns (Qiagen). Each column was washed (4 × 2 ml) with washing buffer [50 mM NaH_2PO_4, 300 mM NaCl, and 10 mM imidazole (pH 8.0)], and the bound proteins were eluted with elution buffer [50 mM NaH_2PO_4, 300 mM NaCl, and 200 mM imidazole (pH 8.0)]. Five 0.6-ml fractions were collected, and LOX activity was assayed. The fractions containing active protein were pooled and desalted using Ecno-Pack® 10 DG columns (Bio-Rad, USA) for further purification by anion-exchange chromatography on a ResourceQ 6-ml column (GE Healthcare, Sweden). The wild-type r-12/15LOX and the mutants were eluted with 20 mM Tris–HCl buffer (either pH 6.8 or pH 8.0) with a linear gradient of NaCl. One-milliliter fractions were collected, and those containing LOX protein (electrophoretic purity ~98%) were pooled and applied for gel filtration on a Superdex™ 200 10/300 GL column (GE Healthcare). Protein was eluted with 20 mM Tris–HCl buffer at pH 6.8 and pH 8.0 either with or without 200 mM NaCl. Protein solutions were concentrated using Spin-X® 6 30,000 MWCO concentrators (Corning, UK) and frozen in 5% (vol) glycerol in liquid nitrogen.

Wild-type hp-12LOX and its seven-point Cys→Ser mutant (7C/S: 89, 140, 199, 221, 378, 508, 656 Cys→Ser) were expressed and purified as described before (the P18054 entry for hp-12LOX in the Swiss-Prot library has been changed to include Met 1; thus, the sequential numbering here is +1 in relation to that previously cited by Aleem *et al.*[12]). Pure proteins (~95% purity) were subjected to gel filtration, and fractions corresponding to the dimers were concentrated in 0.1 M Tris HCl (pH 8) and 0.1 M KCl and frozen (−80 °C) for SAXS analysis. The concentration of each sample was checked before and after SAXS measurements by UV–Vis spectroscopy.

Gel-filtration analysis

The homogeneity of all samples used in this study was checked by gel filtration and native and denaturing gel electrophoreses. For r-12/15LOX, each sample was run on a Superdex™ 200 10/300 GL column (GE Healthcare). To minimize unspecific ionic interaction between the samples and the column material, we selected 20 mM Tris–HCl buffer (pH 6.8) containing 200 mM NaCl at a flow rate of

0.5 ml/min. To estimate the hydrodynamic radius of the samples, we calibrated the column with a gel-filtration calibration kit (Amersham Pharmacia Biotech, Germany) involving catalase (52.2 Å), bovine serum albumin (35.5 Å), and chymotrypsinogen A (20.9 Å). Blue Dextran 2000 was used to determine the column void volume. K_{av} values were calculated using the equation: $K_{av} = (V_e - V_o)/(V_t - V_o)$, where V_e is the elution volume of each protein, V_o is void volume, and V_t is the total bed volume of the column. Finally, the $(-\log K_{av})^{1/2}$ values for standards were plotted *versus* the corresponding hydrodynamic radii (R_h).

Small-angle X-ray scattering

Data collection

The SAXS measurements for r-12/15LOX, its Y614R single mutant and Y98R + Y614R double mutant, and the 7C/S mutant of hp-12LOX were carried out at the EMBL BioSAXS beamline X33 at the DORIS Storage Ring, DESY (Hamburg, Germany),[30] using an X-ray wavelength of 1.54 Å and a sample-to-detector distance of 2.7 m. All samples were measured using a noise-free photon-counting PILATUS detector. Four consecutive frames of 30 s exposure time recorded for each sample were averaged after checking for the absence of radiation-induced protein damage. The scattering patterns of the corresponding buffer solutions were recorded before and after the measurements of the protein sample, and the averaged buffer patterns were subtracted from the protein patterns. A bovine serum albumin solution of 4.2 mg/ml in 50 mM Hepes (pH 7.5) was used for calibrating molecular mass. The samples of 7C/S mutant were kept at 13 °C and measured at two concentrations: 0.5 and 2.8 mg/ml in the presence of 10 mM DTT (to match previous experiments with the wild-type enzyme). To study whether molecular association may account for an increase in molecular particle dimension (radius of gyration R_g), we kept the samples of wild-type rabbit enzyme and its mutants at 10 °C and measured them in the concentration range between 0.5 and 3.0 mg/ml. These measurements were carried out at two pH values (pH 6.8 and pH 8.0) in 20 mM Tris–HCl containing 5% glycerol. For further evaluation, we only considered those samples in which no sizable protein aggregation was detected: (1) pH 6.8: 0.8, 1.6, and 2.9 mg/ml for the wild-type enzyme; 0.5, 0.8, and 0.9 mg/ml for the Y614R mutant; 0.5 mg/ml for the Y98R + Y614R mutant; (2) pH 8.0: 0.7, 1.2, and 2 mg/ml for the wild-type enzyme; 0.4, 1.1, and 2.8 mg/ml for the Y614R mutant; and 1.1 and 2.5 mg/ml for the Y98R + Y614R mutant. (3) To study the impact of salt, we performed measurements for wild-type r-12/15LOX in 20 mM Tris–HCl buffer containing 200 mM NaCl at 2.0 mg/ml (pH 6.8) and at 1.1 and 2.1 mg/ml (pH 8.0).

Data analysis

Data reduction and Guinier analysis were performed using the program PRIMUS.[31] GNOM[32] was used to obtain the maximum size D_{max} and the pair distribution function $p(r)$ of the particle. Preliminary SAXS results for wild-type hp-12LOX had been described before, with the modeling performed to test the possible assembly of molecules into a dimer and with the monomers split into two parts: PLAT domain with residues N_t–108 and the catalytic domain with residues 109–C_t + Fe cofactor.[12] We have used these data for more flexible modeling and for comparison with the enzyme's 7C/S mutant. Low-resolution ab initio models of hp-12LOX wild type (16 Å resolution) and 7C/S mutant (25 Å resolution) were obtained using the program DAMMIF.[33] Six individual runs were performed without symmetry constraints, and the models were averaged to obtain common structural features using the programs DAMAVER and SUPCOMB.[34,35] Rigid-body modeling was performed using the program SASREF.[26] In order to obtain the best fit to the experimental data, we split the dimers into various numbers of the rigid-moving groups (encompassing the following amino acids from conformers A and B): (i) 3 rigid-moving groups—allowing flexibility of only PLAT domains in relation to the combined catalytic parts (A:2–108 | A:109–663 + Fe + B:109–663 + Fe | B:2–108); (ii) 4 rigid-moving groups—allowing movement of the two CAT domains within a dimer in relation to each other (A:2–108 | A:109–663 + Fe | B:109–663 + Fe | B:2–108); (iii) 5 rigid-moving groups (each monomer was split into three rigid groups as in Fig. 2a)—with CAT groups combined and the PLAT and PDZ domains[4] free to move (A:1–108 | A:224–334 | A:109–223 + 335–663 + Fe + B:109–223 + 335–663 + Fe | B:224–334 | B:2–108); and (iv) 6 rigid-moving groups—with independent movement of all parts in the dimer (A:1–108 | A:224–334 | A:109–223 + A335–663 + Fe | B:109–223 + 335–663 + Fe | B:224–334 | B:2–108). The calculations were carried on for the asymmetric (*P*1) dimers consisting of A:A, B:B, and A:B molecules, where molecule A represented 'open' conformation while molecule B represented 'closed' conformation according to the 2P0M model. The breaking points between the domains were chosen arbitrarily at places with great potential for adaptability. The distance between the C^{α} atoms at the junction of the adjacent domains was restricted to be less than 7 Å, while at the dimeric interface, the selected residues were allowed to separate up to 15 Å.

All samples for r-12/15LOX scattered to a resolution of about 30 Å. They were not monodispersive; thus, an improved version of SASREF was used,[26] allowing us to consider polydispersity and free movement of the defined rigid-moving groups. The radius of gyration for the wild-type enzyme was evaluated from the crystal structure (PDB ID: 2P0M) using the program CRYSOL.[36] To assess the volume fractions of the participating solutes of different sizes, we represented each data set by the theoretical scattering profiles calculated from the crystal structure of the monomer and the dimer using the program OLIGOMER.[31] The structure of the monomer was refined using two major domains characterized by the following amino acid numberings: A:2–108, A:109–663 + Fe, and (dimer) A:2–108, A:109–663 + Fe, A109–663 + Fe, A:2–108. During refinement, the catalytic domains (residues 109–663) were fixed at the dimeric interface of A:A to fulfill the program requirement for *P*2 exact symmetry, but approximating that in 2P0M TOP-to-TOP arrangement, while the PLAT domain (residues 2–108) was allowed to move in both monomeric models and dimeric models. The experimental data were fitted by a linear combination of the calculated scattering curves of the monomer and dimer models with appropriate volume fractions.

Thermodynamic stability calculations

In the preparation of the molecular models to be used in SAXS analysis, we have considered molecules of mammalian LOX described in the PDB entries, as well as possible dimers both present in the crystals and theoretically predicted by examination of their potential energy.[12]

The thermodynamic stability of the observed and modeled dimers was evaluated using PSAIA (*P*rotein *S*tructure *a*nd *I*nteraction *A*nalyzer)[37] and PISA (*P*rotein *I*nterfaces, *S*urfaces, and *A*ssemblies).[17] The following dimers were considered: possible dimers in the crystal structures of (1) r-12/15LOX (PDB ID: 2P0M), (2) human engineered 5LOX (PDB ID: 3O8Y), (3) hp-12LOX distorted catalytic domain (PDB ID: 3D3L), and (4) homology models for hp-12LOX formed by A-conformers and B-conformers (observed in PDB ID: 2P0M), including optimization of the interface contacts.

Thermal motion analysis (TLS)

TLS (*t*ranslation, *l*ibration, and *s*crew rotation) was performed for r-12/15LOX using the X-ray coordinates and structure factor files deposited in PDB ID: 2P0M. The TLSMD (*t*ranslation, *l*ibration, and *s*crew rotation *m*otion *d*etection based on crystallographic temperature factor B_i) Web server[38] was used to prepare files for the refinement. Based on the least squares residual *versus* number of TLS segments, the chains of conformers A and B within a dimer were divided into the following rigid-moving groups: conformer A (8 rigid-moving groups), residues 2–47, 48–146, 147–198, 199–240, 241–355, 356–563, 564–601, and 602–663, and conformer B (5 moving groups), residues 2–148, 149–212, 213–549, 550–600, and 601–663. CCP4 (version 6.1) with the program Refmac5 (version 5.5.0066)[39] was used to test the TLS impact on the refinement outcome. The water molecules and inhibitor were removed from the coordinate file, and all *B*-factors were reset to 20 Å^2 prior to the refinement. For better comparison, the structure was refined first without TLS components (no TLS) in two groups for both A and B molecules (TLS 2: residues 2–146 and 147–663 + Fe) and in multiple groups (TLS multi: eight groups for A-conformer, and five groups for B-conformer), as indicated above. The average B was calculated for the same number of residues in the groups compared, regardless of the refinement procedure. Just-deposited h-5LOX (PDB ID: 3O8Y) was analyzed in five groups but not refined.

Acknowledgements

E.S.-J. thanks Dr. Ian Tickle for his helpful discussion of TLS refinement. This study was supported, in part, by DFG (grant GRK 1673) (H.K.); European Molecular Biology Laboratory, Hamburg Outstation, c/o DESY (grants SAXS-09-036 and SAXS-10-004); the European Commission FP6 (E.S.-J. and H.K.); The Frederick M. Douglass Foundation (E.S.-J. and J.J.); and the Frank D. Stranaham Endowment Fund for Oncological Research (J.J.).

References

1. Chen, F. L., Wang, X. Z., Li, J. Y., Yu, J. P., Huang, C. Y. & Chen, Z. X. (2008). 12-Lipoxygenase induces apoptosis of human gastric cancer AGS cells *via* the ERK1/2 signal pathway. *Dig. Dis. Sci.* **53**, 181–187.
2. Dobrian, A. D., Lieb, D. C., Cole, B. K., Taylor-Fishwick, D. A., Chakrabarti, S. K. & Nadler, J. L. (2011). Functional and pathological roles of the 12- and 15-lipoxygenases. *Prog. Lipid Res.* **50**, 115–131.
3. Duroudier, N. P., Tulah, A. S. & Sayers, I. (2009). Leukotriene pathway genetics and pharmacogenetics in allergy. *Allergy*, **64**, 823–839.
4. Jankun, J., Doerks, T., Aleem, A. M., Lysiak-Szydlowska, W. & Skrzypczak-Jankun, E. (2008). Do human lipoxygenases have a PDZ regulatory domain? *Curr. Mol. Med.* **8**, 768–773.
5. Pidgeon, G. P., Lysaght, J., Krishnamoorthy, S., Reynolds, J. V., O'Byrne, K., Nie, D. & Honn, K. V. (2007). Lipoxygenase metabolism: roles in tumor progression and survival. *Cancer Metastasis Rev.* **26**, 503–524.
6. Skrzypczak-Jankun, E., Chorostowska-Wynimko, J., Selman, S. H. & Jankun, J. (2007). Lipoxygenases—a challenging problem in enzyme inhibition. *Curr. Enzyme Inhib.* **3**, 119–132.
7. Gilbert, N. C., Bartlett, S. G., Waight, M. T., Neau, D. B., Boeglin, W. E., Brash, A. R. & Newcomer, M. E. (2011). The structure of human 5-lipoxygenase. *Science*, **331**, 217–219.
8. Notredame, C. (2010). Computing multiple sequence/structure alignments with the T-coffee package.*Curr. Protoc. Bioinf.* 1–25; Chapter 3, Unit 3.8.
9. Dainese, E., Sabatucci, A., van Zadelhoff, G., Angelucci, C. B., Vachette, P., Veldink, G. A. *et al.* (2005). Structural stability of soybean lipoxygenase-1 in solution as probed by small angle X-ray scattering. *J. Mol. Biol.* **349**, 143–152.
10. Mei, G., Di Venere, A., Nicolai, E., Angelucci, C. B., Ivanov, I., Sabatucci, A. *et al.* (2008). Structural properties of plant and mammalian lipoxygenases. Temperature-dependent conformational alterations and membrane binding ability. *Biochemistry*, **47**, 9234–9242.
11. Hammel, M., Walther, M., Prassl, R. & Kühn, H. (2004). Structural flexibility of the N-terminal beta-barrel domain of 15-lipoxygenase-1 probed by small angle X-ray scattering. Functional consequences for activity regulation and membrane binding. *J. Mol. Biol.* **343**, 917–929.
12. Aleem, A. M., Jankun, J., Dignam, J. D., Walther, M., Kuhn, H., Svergun, D. I. & Skrzypczak-Jankun, E. (2008). Human platelet 12-lipoxygenase, new findings about its activity, membrane binding and low-resolution structure. *J. Mol. Biol.* **376**, 193–209.
13. Choi, J., Chon, J. K., Kim, S. & Shin, W. (2008). Conformational flexibility in mammalian 15S-lipoxygenase: reinterpretation of the crystallographic data. *Proteins*, **70**, 1023–1032.
14. Putnam, C. D., Hammel, M., Hura, G. L. & Tainer, J. A. (2007). X-ray solution scattering (SAXS) combined with crystallography and computation: defining accurate macromolecular structures, conformations and assemblies in solution. *Q. Rev. Biophys.* **40**, 191–285.

15. Moin, S. T., Hofer, T. S., Sattar, R. & Haq, Z. (2011). Molecular dynamics simulation of mammalian 15S-lipoxygenase with AMBER force field. *Eur. Biophys. J.* 2011 Mar 1. [Epub ahead of print].
16. Toledo, L., Masgrau, L., Marechal, J. D., Lluch, J. M. & Gonzalez-Lafont, A. (2010). Insights into the mechanism of binding of arachidonic acid to mammalian 15-lipoxygenases. *J. Phys. Chem. B*, **114**, 7037–7046.
17. Krissinel, E. & Henrick, K. (2007). Inference of macromolecular assemblies from crystalline state. *J. Mol. Biol.* **372**, 774–797.
18. Lagarde, M., Croset, M., Authi, K. S. & Crawford, N. (1984). Subcellular localization and some properties of lipoxygenase activity in human blood platelets. *Biochem. J.* **222**, 495–500.
19. Dafforn, T. R. (2007). So how do you know you have a macromolecular complex? *Acta Crystallogr. Sect. D*, **63**, 17–25.
20. Bahadur, R. P., Chakrabarti, P., Rodier, F. & Janin, J. (2004). A dissection of specific and non-specific protein–protein interfaces. *J. Mol. Biol.* **336**, 943–955.
21. Gillmor, S. A., Villasenor, A., Fletterick, R., Sigal, E. & Browner, M. F. (1997). The structure of mammalian 15-lipoxygenase reveals similarity to the lipases and the determinants of substrate specificity. *Nat. Struct. Biol.* **4**, 1003–1009.
22. Skrzypczak-Jankun, E., Borbulevych, O. Y., Zavodszky, M. I., Baranski, M. R., Padmanabhan, K., Petricek, V. & Jankun, J. (2006). Effect of crystal freezing and small-molecule binding on internal cavity size in a large protein: X-ray and docking studies of lipoxygenase at ambient and low temperature at 2.0 Å resolution. *Acta Crystallogr. Sect. D*, **62**, 766–775.
23. Aleem, A. M., Wells, L., Jankun, J., Walther, M., Kuhn, H., Reinartz, J. & Skrzypczak-Jankun, E. (2009). Human platelet 12-lipoxygenase: naturally occurring Q261/R261 variants and N544L mutant show altered activity but unaffected substrate binding and membrane association behavior. *Int. J. Mol. Med.* **24**, 759–764.
24. Zhang, M., Windheim, M., Roe, S. M., Peggie, M., Cohen, P., Prodromou, C. & Pearl, L. H. (2005). Chaperoned ubiquitylation—crystal structures of the CHIP U box E3 ubiquitin ligase and a CHIP–Ubc13–Uev1a complex. *Mol. Cell*, **20**, 525–538.
25. Murzin, A. G. (2008). Biochemistry. Metamorphic proteins. *Science*, **320**, 1725–1726.
26. Petoukhov, M. V. & Svergun, D. I. (2005). Global rigid body modelling of macromolecular complexes against small-angle scattering data. *Biophys. J.* **89**, 1237–1250.
27. Wecksler, A. T., Jacquot, C., van der Donk, W. A. & Holman, T. R. (2009). Mechanistic investigations of human reticulocyte 15- and platelet 12-lipoxygenases with arachidonic acid. *Biochemistry*, **48**, 6259–6267.
28. Wecksler, A. T., Kenyon, V., Garcia, N. K., Deschamps, J. D., van der Donk, W. A. & Holman, T. R. (2009). Kinetic and structural investigations of the allosteric site in human epithelial 15-lipoxygenase-2. *Biochemistry*, **48**, 8721–8730.
29. Walther, M., Anton, M., Wiedmann, M., Fletterick, R. & Kuhn, H. (2002). The N-terminal domain of the reticulocyte-type 15-lipoxygenase is not essential for enzymatic activity but contains determinants for membrane binding. *J. Biol. Chem.* **277**, 27360–27366.
30. Roessle, M. W., Klaering, R., Ristau, U., Robrahn, B., Jahn, D., Gehrmann, T. *et al.* (2007). Upgrade of the small-angle X-ray scattering beamline X33 at the European Molecular Biology Laboratory, Hamburg. *J. Appl. Crystallogr.* **40**, s190–s194.
31. Konarev, P. V., Volkov, V. V., Sokolova, A. V., Koch, M. H. J. & Svergun, D. I. (2003). PRIMUS—a Windows-PC based system for small-angle scattering data analysis. *J. Appl. Crystallogr.* **36**, 1277–1282.
32. Semenyuk, A. V. & Svergun, D. I. (1991). GNOM—a program package for small-angle scattering data processing. *J. Appl. Crystallogr.* **24**, 537–540.
33. Franke, D. & Svergun, D. I. (2009). DAMMIF, a program for rapid ab-initio shape determination in small-angle scattering. *J. Appl. Crystallogr.* **42**, 342–346.
34. Kozin, M. B. & Svergun, D. I. (2001). Automated matching of high- and low-resolution structural models. *J. Appl. Crystallogr.* **34**, 33–41.
35. Volkov, V. V. & Svergun, D. I. (2003). Uniqueness of ab initio shape determination in small angle scattering. *J. Appl. Crystallogr.* **36**, 860–864.
36. Svergun, D. I., Barberato, C. & Koch, M. H. J. (1995). CRYSOL—a program to evaluate X-ray solution scattering of biological macromolecules from atomic coordinates. *J. Appl. Crystallogr.* **28**, 768–773.
37. Mihel, J., Sikic, M., Tomic, S., Jeren, B. & Vlahovicek, K. (2008). PSAIA—Protein Structure and Interaction Analyzer. *BMC Struct. Biol.* **8**, 21.
38. Painter, J. & Merritt, E. A. (2006). TLSMD Web server for the generation of multi-group TLS models. *J. Appl. Crystallogr.* **39**, 109–111.
39. CCP4 (1994). The CCP4 suite: programs for protein crystallography. *Acta Crystallogr. Sect. D*, **50**, 760–763.